Dynamics of rising CO_2 bubble plumes in the QICS field experiment Part 1 – The experiment

Nazmi Sellami [a,b], Marius Dewar [a], Henrik Stahl [c,d], Baixin Chen [a,*]

[a] Institute of Mechanical, Process and Energy Engineering, School of Engineering & Physical Sciences, Heriot-Watt University, Riccarton, Edinburgh, EH14 4AS, United Kingdom
[b] Environment and Sustainability Institute, University of Exeter, Penryn Campus, Penryn, TR10 9FE United Kingdom
[c] Scottish Association for Marine Science, Scottish Marine Institute, Oban, Argyll, PA37 1QA, United Kingdom
[d] Department of Natural Science and Public Health, Zayed University, PO Box 19282, Dubai, United Arab Emirates

ARTICLE INFO

ABSTRACT

The dynamic characteristics of CO_2 bubbles in Scottish seawater are investigated through observational data obtained from the QICS project. Images of the leaked CO_2 bubble plume rising in the seawater were captured. This observation made it possible to discuss the dynamics of the CO_2 bubbles in plumes leaked in seawater from the sediments. Utilising ImageJ, an image processing program, the underwater recorded videos were analysed to measure the size and velocity of the CO_2 bubbles individually. It was found that most of the bubbles deform to non-spherical bubbles and the measured equivalent diameters of the CO_2 bubbles observed near the sea bed are to be between 2 and 12 mm. The data processed from the videos showed that the velocities of 75% of the leaked CO_2 bubbles in the plume are in the interval 25–40 cm/s with Reynolds numbers (Re) 500–3500, which are relatively higher than those of an individual bubble in quiescent water. The drag coefficient C_d is compared with numerous laboratory investigations, where agreement was found between the laboratory and the QICS experimental results with variations mainly due to the plume induced vertical velocity component of the seawater current and the interactions between the CO_2 bubbles (breakup and coalescence). The breakup of the CO_2 bubbles has been characterised and defined by Eötvös number, *Eo*, and *Re*.

1. Introduction

In addition to the carbon emission trading (TradeXchange, 2013), another potential solution to mitigate greenhouse gases release to the atmosphere and to meet the obligations specified by the Kyoto Protocol, is the disposal of carbon dioxide (CO_2) in the deep geoformations or the ocean (Freund and Ormerod, 1997), which was first proposed by Marchetti (1977). This process is known as carbon capture and storage (CCS) by which CO_2 is captured from power plants and industrial sources, before it is emitted into the atmosphere, and then injected into deep sub-seabed reservoirs/geological structures for permanent storage (Han et al., 2012).

The greatest concern on performing CCS in the engineering scale, is the risk of leakage from storage sites, it is therefore necessary to investigate the leakage possibility and the impacts of any potential CO_2 leakage on the environment, especially on the marine life for under seabed storage (Noble et al., 2012). Dispersion and dissolution of CO_2 bubbles in seawater are of special interest from the

biological point of view, because of its importance in the changes of water quality.

In order to study the effects of a potential leak from a carbon under seabed storage on the UK marine environment, the Quantifying and Monitoring Potential Ecosystem Impacts of Geological Carbon Storage (QICS) project, was launched in 2010 (Blackford et al., 2014). QICS is a scientific research project involving a field experiment of injection of CO_2 into shallow marine sediments. One of the main objectives of the project, in addition to the development of monitoring and observation methods, is to generate experimental data to calibrate and develop models for predicting the change in pH or pCO_2 of the seawater in and above the sediments from leaked CO_2. The changes in pH (or pCO_2) are vital data for the biogeochemical and ecological models in order to predict the impact of CO_2 leakages on the marine biological system in a variety of situations. Sufficient understanding of CO_2 bubble rising and dissolution characteristics in a plume are necessary and fundamental to the development of two-phase plume models for simulation of the changes in the seawater. In addition to the small-scale ocean turbulent model and bubble dissolution model, the two-phase plume model requires two key parameters which are: (i) the
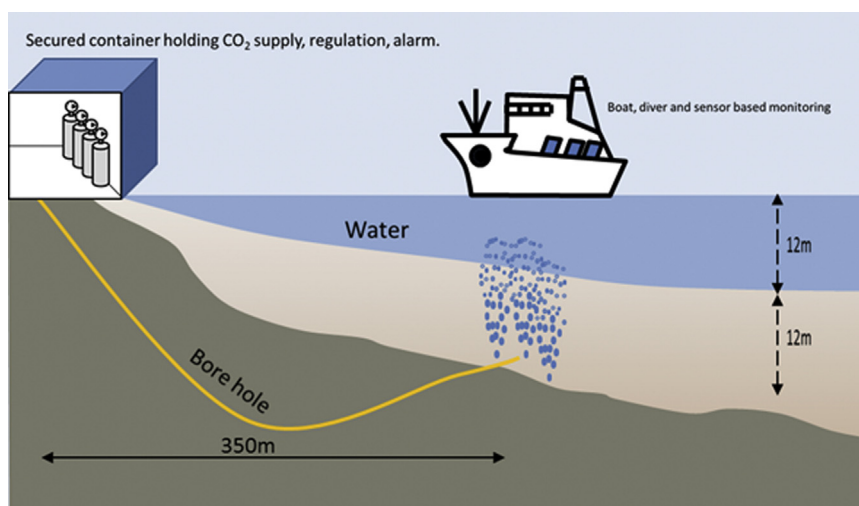
Fig. 1. Schematic of QICS CO_2 release experiment.

initial CO_2 bubble size and leakage flux to be used as input and (ii) a correlation of the drag coefficient as function of the CO_2 bubble Reynolds number as it dominates the rise velocity and distance of the bubbles. By precisely measuring the size of the CO_2 bubbles and the rising velocities, these two parameters can be established.

The prediction of the dispersion of CO_2 bubbles has been attempted by numerical models (Chen et al., 2005, 2009; Dewar et al., 2013). Numerous experimental studies aimed at determining the drag coefficient correlation of gas bubble or liquid droplet as function of Reynolds numbers have been carried out, which had been summarised by Clift et al. (1978). Bozzano and Dente (2001) proposed a different correlation of drag coefficient as function of a group of dimensionless parameters of Reynolds number (Re), Morton numbers (Mo) and Eötvös number (Eo) of a single gas bubble or liquid droplet rising into a liquid phase (the details of the definitions of those dimensionless parameters can be found in Section 3, Eqs. (3)–(5)). Bozzano and Dente (2001) described the comparison between their correlation and experimental data as satisfactory. Rodrigue (2001) developed a generalised correlation for the motion of single gas bubble in high viscosity Newtonian fluids. The correlation was compared with the previous experimental literature data for a broad range of Morton numbers. It was found that the correlation showed a good agreement for highly viscous fluids ($Mo > 10^{-8}$). Kelbaliyev (2011) presented an extensive review of twelve developed correlations of drag coefficient for a wide Re range up to 10^6. All of the correlations were studied for single bubble rising in Newtonian fluids and developed for various ranges of a group of dimensionless parameters. The dynamics of the CO_2 bubble with the existence of other CO_2 bubbles in the near environment (CO_2 plume), however, differs notably from the one of an isolated bubble due to bubble interactions and the interactions between bubbles and water in the plume. In this work we report the results from observing the dynamics of CO_2 bubbles rising freely in a plume, created in the QICS field experiment (Blackford et al., 2014). It should be noted that, in addition to the free rising bubbles and plumes, the dynamics of bubble flows in pipes have been extensively investigated and the results obtained from those studies, can be the references of the studies of CO_2 plumes developed in the ocean. Details of the predictions of void fraction and heat transfer characteristics in two-phase systems can be found from recently published paper by Brooks et al. (2012).

The development of the drag coefficient correlation requires experimental data of the velocity and correspondent sizes and geometries of the rising gas bubbles in the fluids. Most of the previous studies have used cameras to gather these data; the motion of a single bubble was investigated experimentally using a camera to follow the rising bubbles (Zhang et al., 2008). Bando and Takemura (2006) used CCD (charge-coupled device) cameras to study the behaviour of carbon dioxide sphere rising in fluids, Takemura and Yabe (1999) used CCD cameras to study the rising speed and dissolution rate of CO_2 bubbles in slightly contaminated water, Zhang et al. (2012) used high speed cameras to study the multi-bubble behaviour in carbon capture system with ionic liquid, Brewer et al. (2002) used HDTV (High Definition Television) cameras and ROV (Remotely Operated Vehicles) in the field to measure the rise rate and dissolution rate of freely released CO_2 droplets in deep ocean, Luke and Cheng (2006) used high speed cameras to study the bubble formation with pool boiling, Zaruba et al. (2005) used CCD cameras to study the bubble motion in a rectangular bubble column, and many others (Wang and Dong, 2008; Luther et al., 2004; Bian et al., 2011; Wang and Dong, 2009; Hongyi and Feng, 2009) have used video cameras to study the velocity and size of a bubble rise in a liquid column.

In this paper, the dynamics of leaked CO_2 bubbles in a plume in the Scottish seawater are studied experimentally using video recordings. The experiment was carried in the ocean by creating a leakage scenario 12 m beneath the sediment and capturing video sequences of rising CO_2 bubbles reaching the seawater.

2. Experimental method

The QICS experiment is novel, in that for the first time CO_2 was injected into a natural system in a way that would closely mimic CO_2 leakage. The CO_2 release experiment was carried out under the Scottish sea at Ardmucknish Bay (56 29.55 N, 05 25.71 W) by drilling a borehole 12 m deep underlying the sandy mud sediments as illustrated in Fig. 1. The release of the CO_2 was controlled and monitored from a mobile laboratory at a nearby site after seeking the permission from the government and local authorities. The experiment was conducted by the Scottish Associations for Marine Science (SAMS) laboratory, near Oban in Western Scotland. After the migration of the CO_2 released in the sediment where part of it was dispersed and dissolved, the CO_2 reaches the seabed in gas bubble phase at 9–12 m water depth.

The motions of the CO_2 bubbles were captured using high-definition (HD) video system to investigate the rise of CO_2 bubbles in seawater. A HDTV Canon EOS 5D Mark II video camera was used to track the rising CO_2 bubbles with a frame rate 30 fps (frames per second) producing digital HD images with resolution 1080 pixels vertically and 1920 pixels horizontally per frame. The elevation of
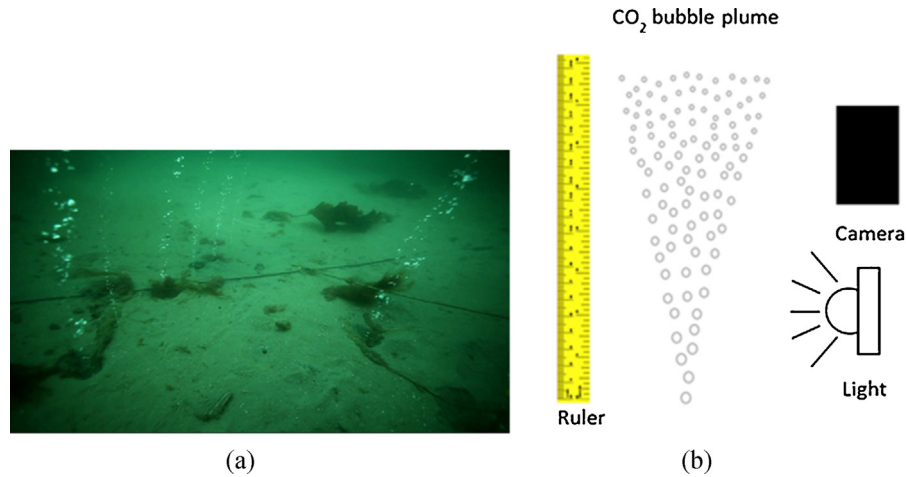
Fig. 2. Experimental set-up: (a) The observation field of multi-bubble-plumes. (b) Schematic view of the observation system.

the camera is approximately 20 cm above the sea floor. A ruler has been aligned with the CO_2 bubble plume as a referential dimension. The rising CO_2 bubbles were exposed to a green light during the capturing of the video as illustrated in Fig. 2.

The physical properties at ambient temperature of the seawater (10.8 °C) and CO_2 bubbles are reported in Table 1.

3. Rising CO_2 bubbles video processing

There is a direct analytical relationship between the drag coefficient (C_d) and the CO_2 bubble velocity (Dewar et al., 2013). To find this relationship, the experimental sizes and shapes of the CO_2 bubbles and the correspondent velocity are acquired. A method was developed that allowed the measurement of the CO_2 bubble sizes, velocities and their distributions. The bubble trajectories and the interactions among the CO_2 bubbles were investigated by analysing the videos recorded using the underwater digital video camera; the videos were processed using image processing software ImageJ (Schneider et al., 2012). The locations and the edge of the CO_2 bubble surfaces were determined as a result of manual image processing of each frame of the video separately. An edge contour was sketched around each bubble studied with the help of ImageJ to detect the cross-sectional area of the CO_2 bubble. A sample of the image of the bubble and the results are illustrated in Fig. 3.

For small CO_2 bubbles, their sizes can be more accurately measured since the bubble is almost spherical in shape, except where they are less than 2 mm where the resolution is too poor to conduct measurements. When the CO_2 bubbles are large, they take the shape of a perfect ellipsoidal or wobbling ellipsoidal
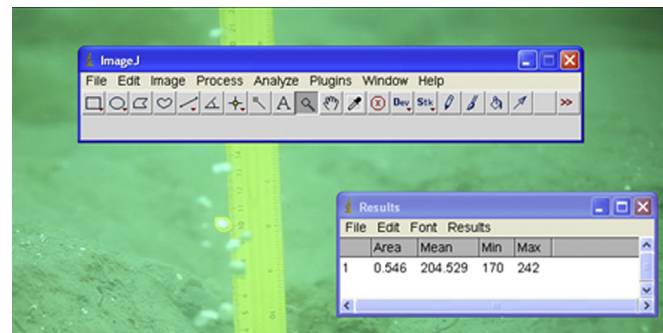
shape; the evaluation of the size is characterised by an equivalent diameter (d_e). The CO_2 bubbles equivalent diameter is defined as the diameter of an equivalent sphere with the same bubble area of the equivalent CO_2 bubbles:

$$d_e = \sqrt{\frac{4A}{\pi}} \qquad (1)$$

where A is the measured area of the CO_2 bubble. It has been noted that the images taken from the video are two-dimensional vertical sections of the bubble, therefore, the measured area, A, is the vertical cross-sectional area of the bubble. The geometry of the large CO_2 bubbles studied is characterised by two dimensions: the major axis dimension (D_{mj}) and the minor axis diameter (D_{mi}) of the vertical cross section. In this study the unit of bubble size, including d_e, D_{mi} and D_{mj}, are generally in metre if not specified.

The vertical movement of CO_2 bubbles were measured. Consider two successive frames taken from the record video, the coordinates of the CO_2 bubbles in the first frame and second frame are y_1 (m) and y_2 (m) respectively. The time interval between the two fames is Δt (=1/30 s). Then the velocity vertical velocity, V (m/s), of the CO_2 bubble is calculated by

$$V = \frac{(y_2 - y_1)}{\Delta t} \qquad (2)$$

It has been noted that the velocity measured by Eq. (2) is the 'gross' velocity, rather than the relative velocity of the CO_2 bubble to that of seawater. Such a 'gross' velocity measured from the field observations can be defined as the velocity integrated with the seawater background velocity (current and tides) and plume velocities generated by the interactions between seawater and bubbles, and among the bubbles themselves. The effects of these factors on the bubble rising velocity and drag coefficient will be discussed in Section 4.2, in comparison with that of a single rising bubble in quiescent water. The dimensionless numbers used in this study to characterise the motion and shape of the CO_2 bubbles are: Reynolds number (Re), Eötvös number (Eo), and Morton number (Mo), which are defined as,

$$Re = \frac{\rho_w V d_e}{\mu_w} \qquad (3)$$

where μ_w (Pa s) is the dynamic viscosity of the seawater and ρ_w (kg/m^3) is the seawater density.

$$Eo = \frac{\rho_w g d_e^2}{\sigma} \qquad (4)$$

Fig. 3. A sample of the image of the bubble and measurement of CO_2 bubble size.

Table 1
Physical properties of the selected fluids at 10 °C.

Properties		Seawater	CO_2
Dynamic viscosity (mPa s)	μ_w	1.4 (Schetz and Fuhs, 1999)	14.2 (National Bureau of Standards, 1960)
Interfacial tension (N/m)	σ	7.37×10^{-2} (Chun and Wilkinson, 1995)	
Density (kg/m^3)	ρ	1027 (Unesco, 1981)	1.9 (Ito, 1984)
Measured salinity (ppt)	S	33.7	–

where g (m/s^2) is gravitational acceleration and σ (N/m) is the interfacial tension between the water and the CO_2 gas.

$$Mo = \frac{gV^4(\rho_w - \rho_{CO_2})}{\rho_w^2 \sigma^3} \tag{5}$$

where ρ_{CO_2} (kg/m^3) is the density of the CO_2. The data of physical properties of seawater and CO_2 in the field conditions can be found from Table 1.

The data obtained from the directly observations, such as the 'gross' velocity and the bubble size are referred to as the raw data in this study, in order to distinguish the data obtained with corrections.

4. Results and discussion

The CO_2 bubbles were studied up to 30 cm from sea floor at their initial states when they leak from the sediments into the seawater. The velocities (V) and sizes (d_e) of the bubbles have been recorded to generate the results to be discussed in this section.

It was found from the data obtained by the experiment, as shown in Fig. 4, that the size of the leaked CO_2 bubbles varies between 0.2 and 1.2 cm with a correspondent velocity varying between 20 cm/s and 45 cm/s.

4.1. Distributions of bubble size and velocity

The size of the CO_2 bubbles is the key parameter for the dynamics of free rising bubbles, including the dispersion and dissolution. The larger the bubble, the further it will travel in the seawater and the longer it will take to dissolve. For this reason, the distribution of the initial bubble size is vital data for the model prediction of the height travelled by the CO_2 bubbles in the water column before dissolving, as well as the changes in pH and pCO$_2$ of the water to be created, for which the details have been modelled and discussed in the second part of the paper (Dewar et al., 2014). It was found from QICS field experiment that more than 50% of the leaked CO_2 bubbles have a d_e varying between 0.65 cm and 0.9 cm, with only
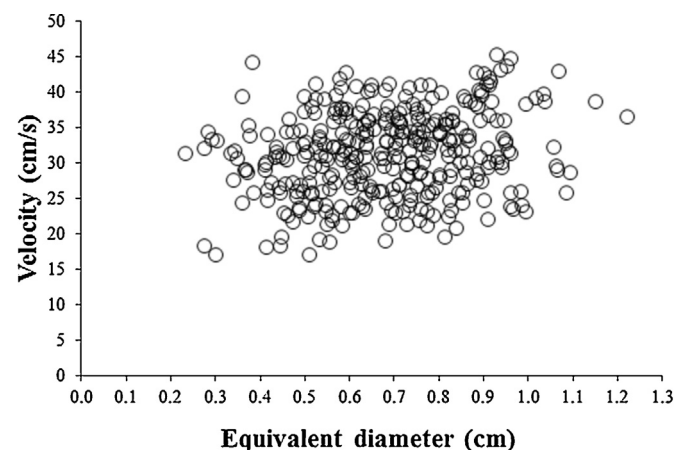
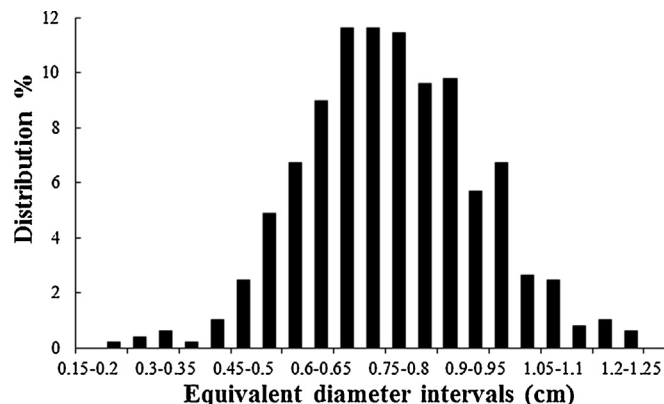**Fig. 5.** Observed size distribution of leaked CO_2 bubbles.

a low presence (<1.5%) of both the small bubbles ($d_e < 0.4$ cm) and large bubbles ($d_e > 1.1$ cm), respectively. The bubbles, after migrating from the sediment to the seawater, have the distribution of the different sizes as illustrated in Fig. 5 which has been used in the bubble plume modelling to set the initial bubble size (Dewar et al., 2014).

Another important parameter of the free rising CO_2 bubbles is the rising velocity. It was found, as illustrated in Fig. 6, the distribution of the leaked CO_2 bubble velocities, that most of the CO_2 bubbles (>75%) rise with a velocity between 25 cm/s and 40 cm/s, again we would like to highlight that these are the "gross" rising velocities of bubbles in the plume, which are detected directly by the video images, rather than the relative rising velocities of bubbles to the seawater.

4.2. The drag coefficient of leaked CO_2 bubbles

The drag coefficients of the leaked CO_2 bubbles are calculated by assuming the rising velocity measured being the terminal velocity. For bubbles rising freely in the seawater, the forces acting on the bubbles are mainly buoyancy and drag force. Taking into
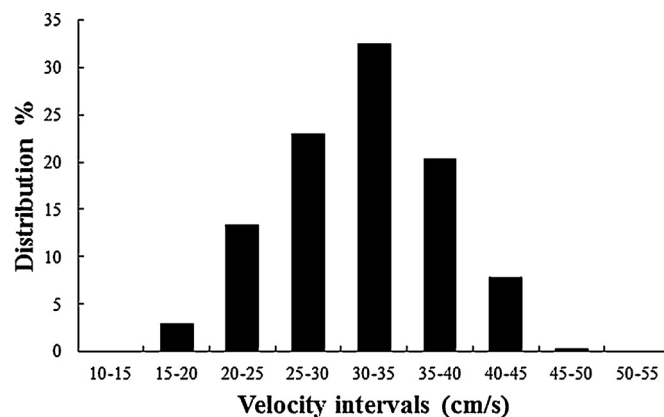
Fig. 4. The distribution of sizes and velocity of leaked CO_2 bubbles measured directly from videos.

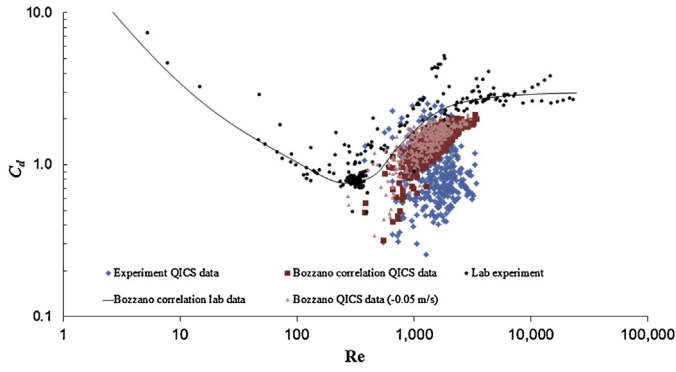**Fig. 6.** Observed velocity distribution of CO_2 bubbles.

Fig. 7. Comparison of drag coefficient correlation (Bozzano and Dente, 2001) with lab. experiment data (black markers) (Dewar et al., 2013) and the data from QICS experiment directly by Eq. (7) (blue markers) and the data from QICS experiment by Eqs. (8)–(10) (dark red markers) and with the corrected velocities of plume induced velocity (light red markers).

consideration the equilibrium of the buoyancy and drag force, the equation of motion for the CO_2 bubble can be written as

$$\frac{\pi d_e^3}{6}(\rho_w - \rho_{CO_2})g = \frac{1}{2}C_d \rho_w V^2 \frac{\pi d_e^2}{4} \tag{6}$$

The density of the CO_2 gas can be negligible in comparison with the density of the seawater; therefore $\rho_w - \rho_{CO_2} \approx \rho_w$. The incorporation of this assumption into Eq. (6) gives the drag coefficient C_d of the CO_2 bubbles as,

$$C_d = \frac{4gd_e}{3V^2} \tag{7}$$

Using Eqs. (7) and (3), the drag coefficient C_d and the Reynolds number Re were calculated for the studied CO_2 bubbles by using the observed velocity (V). The relationship between the C_d and the Re obtained from the QICS experiment by the raw data is shown in Fig. 7 in blue markers, along with the drag coefficient results of methane gas bubbles obtained from the experimental study carried out in laboratory (Dewar et al., 2013) shown in black solid markers. It was found that only a few of the CO_2 bubbles studied within the QICS experiment match with the laboratory results for the Re range between 500 and 3500. Meanwhile, the data from QICS field experiment are broadly diverse and the majority of the QICS CO_2 bubbles had a variation of the C_d between 0.4 and 2.3 for the same Re number which is relative smaller than those of an individual bubble. The difference can be explained due to three major factors. The first factor considered in the QICS experiment results in the variation of the C_d is due to the CO_2 bubbles studied rising in a plume of bubbles compared to individual bubbles studied in the laboratory experiments. In the QICS experiment, the velocity of the CO_2 bubbles measured is the absolute ('gross') velocity of the bubbles carried by the water plume, for which, the effects vary depending on the location of the CO_2 bubbles in the plume, where the larger the velocity approaching to the centre of the plume. In general, the absolute velocity of bubbles in the plume is larger than the relative velocity of bubble to the water, which leads to a relatively smaller C_d. Also providing the variation in the drag coefficient, as the same size CO_2 bubbles can have different velocities depending on its position in the plume (Domingos and Cardoso, 2013). The second factor that should be considered is the effects from the interactions among the CO_2 bubbles studied in the QICS experiment. It is detected from the observation data that the larger bubbles breakup as rising, meanwhile, coalescence of two or more CO_2 bubbles also occurs. The interactions change the velocity of the CO_2 bubbles due to the exchanges in momentum and the difference in sizes from the attraction or collision of the CO_2 bubbles (Liao and Lucas, 2009).

The third factor is the presence of the vertical component of the seawater tidal velocity.

In order to examine the effects from the seawater plume on the individual bubble dynamics, two-phase plume model simulations were carried out in part 2 of this study (Dewar et al., 2014) and it was found that the seawater in the plume is rising at velocities ranging from 3.5 cm/s to 5.0 cm/s in the centre of the plume, which results from the interactions between the momentum transferred by the rising bubbles and that of pealing down due to the increasing of density of CO_2 solution. This plume background seawater velocity data ($V_s = 3.5$–5.0 cm/s) is used to estimate the relative velocities of observed bubbles (V_r), $V_r = V - V_s$, where V is the bubble rising velocity observed from field experiment and shown in Fig. 4.

The effect of bubble deformation is then investigated by employing the correlations proposed by Bozzano and Dente (2001). In general, the drag coefficient C_d of a spherical bubble can be expressed by the Reynolds numbers (Sommerfeld et al., 2010) alone, for which the correlations were proposed (Kelbaliyev, 2011). For large and deformable bubbles, however, the effect from flows generated by changes in shape of bubbles on the drag coefficient must be taken into account. In practice, additional dimensionless parameters, Morton number, Mo, and Eötvös number, Eo, are used for construction of the correlations (Bozzano and Dente, 2001), which is represented with the solid line in Fig. 7. The correlation is defined as:

$$C_d = f \left(\frac{D_{mj}}{d_e}\right)^2 \tag{8}$$

$$f = \frac{48}{Re}\left(\frac{1 + 12M^{1/3}}{1 + 36M^{1/3}}\right) + 0.9\frac{Eo^{3/2}}{1.4(1 + 30M^{1/6}) + Eo^{3/2}} \tag{9}$$

$$\left(\frac{D_{mj}}{d_e}\right)^2 = \frac{10(1 + 1.3M^{1/6}) + 3.1Eo}{10(1 + 1.3M^{1/6}) + Eo} \tag{10}$$

The correlation is tested by using the data of bubbles equivalent diameters d_e and the corresponding velocities from the QICS experiment for calculation of the dimensionless parameters, Re, Eo, and Mo.

As shown in Fig. 7, in comparison with the raw data (blue markers), the effect of bubble deformation on the drag coefficient of plume bubbles is predicted (dark red markers) estimated from the correlation Eqs. (8)–(10), using experimental data of d_e and V. The deformation of bubbles generates a larger drag force, for which cannot directly detected by the raw data using Eq. (7). The light red markers in Fig. 7 are data representing the effects of induced seawater velocity on the estimation of the drag coefficient, calculated from correlation Eqs. (8)–(10) and data of d_e and the corrected rising velocity V_r. It seems that the effects of bubble deformation are dominate in comparison with that of the induced seawater velocity, which is relatively smaller than the velocity of the bubbles observed in the field experiment.

Although the data are still divergent with a difference observed, in general, with that predicted by the correlation without using the QICS data (solid line). The divergent data are due to the results of the variable velocities at a given bubble equivalent diameter (refer to Fig. 5) as discussed in the first part of this section. It can be found from the results that in comparison with the results using Eq. (7), the corrected data are more approaching to those from laboratory experiments and the correlation (Bozzano and Dente, 2001) from the individual bubble rising in the quiescent water. The effects from the plume on the individual bubble rising dynamics are demonstrated, meanwhile, it is also demonstrated that the correlation proposed by Bozzano and Dente (2001) is applicable to the relative dilute bubbly plume simulations.
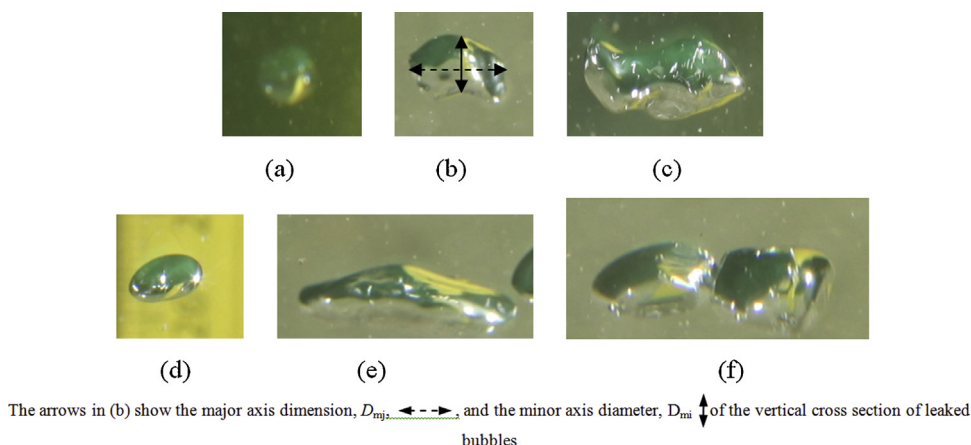
The arrows in (b) show the major axis dimension, D_{mj}, ◄- - -►, and the minor axis diameter, D_{mi} ↕ of the vertical cross section of leaked bubbles

Fig. 8. Different shape of CO_2 bubbles: (a) spherical, (b) cap shape, (c) ellipsoidal wobbling, (d) ellipsoidal, (e) before breakup and (f) breakup moment.

There is another factor that should be taken into account when the comparisons with the laboratory experimental results (Dewar et al., 2013), which is the effects from dissolution. The available data (Dewar et al., 2013) are from methane bubbles, which are almost insoluble in the water, whereas the field experimental results are from CO_2 bubbles with relative large solubility. This effect should be investigated individually by well-designed lab. experiments or numerical simulations.

4.3. CO_2 bubbles shape characterisation

Considering the important effects of the shapes on the drag coefficient and further the dissolution rate, the data obtained from QICS experiment are analysed for investigation of the geometric characterisation of the different CO_2 bubbles in the open seawater.

Different CO_2 bubbles shapes were observed in the seawater during the QICS experiment. Fig. 8 shows photos captured of the six typical shapes of the bubbles, two of them characterising the breakup moment when the bubbles are about to divide (Fig. 8(e)) and breaking up in two (Fig. 8(f)). The CO_2 bubble shapes can be categorised into types of spherical (small size), cap and ellipsoidal shape, and ellipsoidal wobbling shape (large size).

The characteristics of bubbles deformation can be discussed by using Eötvös and Reynolds numbers. It can be found from the data retreated from recorded videos of CO_2 bubbles leaked in the QICS experiment in the $Eo–Re$ diagram, shown in Fig. 9, that the different bubble shapes can be characterised. When $Eo < 2$, the CO_2 bubbles are small and have spherical shapes; $2 < Eo < 7$, the CO_2

bubbles have ellipsoidal shapes; and $Eo > 7$ the CO_2 bubbles have ellipsoidal wobbling shapes.

Experiment data shows that the wobbling CO_2 bubbles were potentially going towards two possible shape situations: breakup into two smaller bubbles or becoming stable into a perfect ellipsoidal shape after losing part of its volume due to dissolution in seawater.

The diameter considered in the calculation of the Reynolds numbers is the equivalent diameter (d_e), however, as can be seen in Fig. 8, the CO_2 bubbles with the same d_e have different widths expressed by the major axis dimension (D_{mj}). As have been discussed by Brooks et al. (2012), the major axis dimension (D_{mj}) is a parameter that characterises the bubble breakup. From QICS experiment, the data identify clearly when $d_e > 0.5$ cm, as in Fig. 10, a good liner relation is shown between the equivalent diameter of the CO_2 bubbles and their major axis, with a gradient of 1.82,

$$D_{mj} = \begin{cases} d_e & \text{if } d_e \le 0.5 \text{ cm} \\ 1.82d_e - 0.4 & \text{if } d_e > 0.5 \text{ cm} \end{cases} \quad (11)$$

where D_{mj} and d_e both are in cm.

This relation is suggested to represent the parameter for characterising the breakup in the numerical modelling as the CO_2 bubbles stretch horizontally before breaking up.
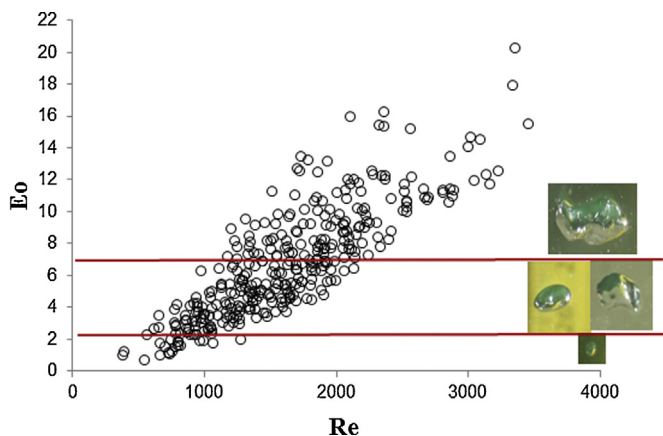

Fig. 9. Characterisation of the CO_2 bubble shapes observed from QICS experiment.
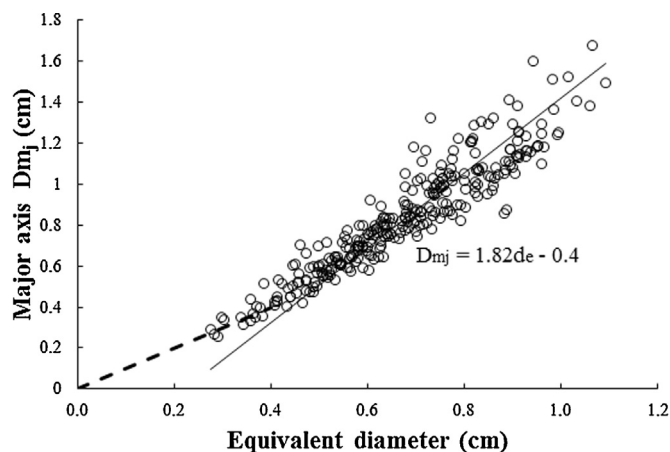

Fig. 10. The relation between major axis of the bubbles (D_{mj}) and the equivalent diameter (d_e) from QICS experiment (the symbols) and the liner equation (solid line).
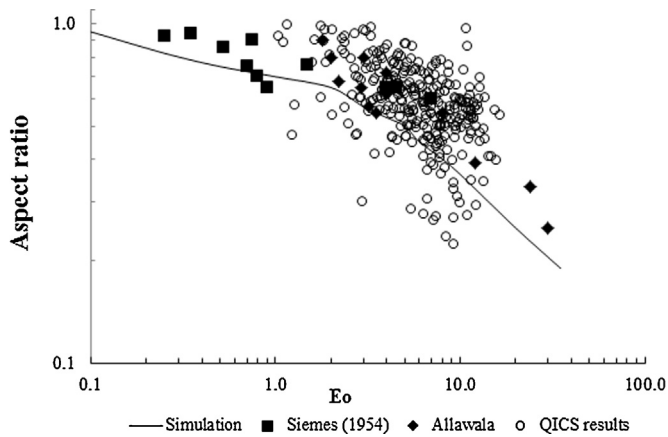
The CO_2 bubble shape can be characterised, in another way, by the aspect ratio as defined as,

$$A_r = \frac{D_{mi}}{D_{mj}} \tag{12}$$

Since the Eo number is the ratio of buoyancy force to interfacial tension, the parameter in the determination of bubble shape, the aspect ratio is examined against the Eo as illustrated in Fig. 11. It shows, that the aspect ratio decreases with Eo increases, the larger buoyancy force enhances the deformation of the bubbles to create a large width. In comparison with lab. experiment data, it shows a good agreement of the QICS results (circles in Fig. 11) with the experimental results and simulation presented by Bozzano and Dente (2001), thus validating the use of Eo to characterise the shapes of the CO_2 bubbles.

4.4. Interaction of CO_2 bubbles in seawater

From the processing of the videos filmed during the QICS experiment, interactions between the CO_2 bubbles have been observed. The interaction occurs as breakup of some of the large CO_2 bubbles which reduce their size and therefore velocity or coalescence between two CO_2 bubbles to give birth to a larger CO_2 bubble with higher velocity.

The example of the CO_2 bubble breakup, as shown in Fig. 12, observed in the QICS experiment captured videos. It can be seen
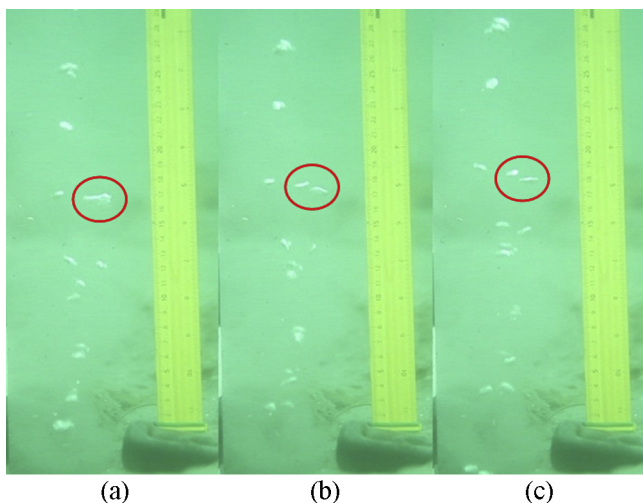

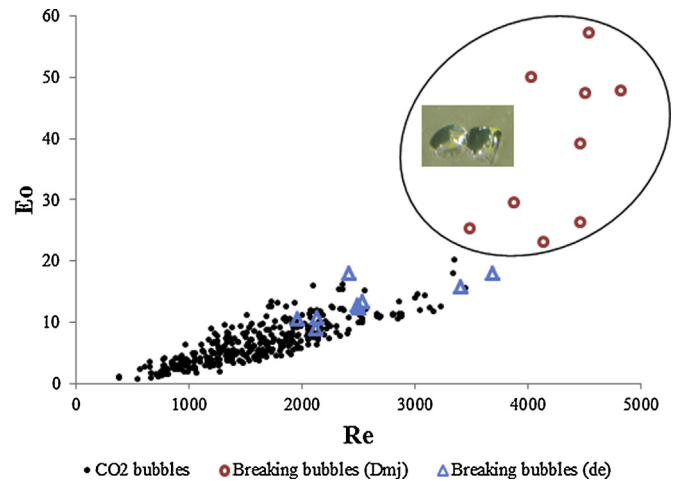**Fig. 12.** Photo montage of CO_2 bubble breakup.

Fig. 13. Eo (Eo_b) – Re (Re_b) diagram of CO_2 bubble breakup.

that the CO_2 bubble in the first photo (Fig. 12(a)) circled with red reached a large D_{mj} before breaking into two CO_2 bubbles as showing in the two following photos (Fig. 12(b) and (c)).

The clearest breakups of the CO_2 bubbles have been selected and illustrated with the green triangles in Fig. 13 represented in the Eo–Re diagram. From the data in the Eo–Re diagram, it seems that the bubbles that experience break-up (the blue triangle) are hard to be differentiated from the other rising bubbles as the data shows they all fit a smooth trains. In order to indicate the breaking bubbles, it was proposed that the Eo and Re should be defined by using the major dimension, D_{mj}, instead of the equivalent diameter, d_e. By this definition, Eötvös number as Eo_b and Reynolds number as Re_b, as shown by the red circles in Fig. 13, the breaking bubbles are clearly identified. It can be concluded that the breakup occurs for the CO_2 bubbles when $Eo_b > 20$ and $Re_b > 3500$. For modelling of the breakup in the two-phase plume modelling in part 2 of this study (Dewar et al., 2014), Eq. (12) can be used to calculate the D_{mj} of CO_2 bubbles for estimating the breakup Eötvös number and Reynolds number.

In addition to the CO_2 bubbles breakup, coalescence between bubbles has been observed at a frequency of 2.5 coalescences every second at the first 30 cm high above the sea floor. When the CO_2 bubbles coalesce, they form a larger bubble that will take longer to dissolute in the seawater. The data of bubbles coalescence frequency of 2.5 (Hz) observed from QICS experiment can be the reference value to develop the bubbles coalescence models for plume simulations in part 2 of this study (Dewar et al., 2014).

5. Conclusion

The dynamics of rising CO_2 bubbles in the Scottish seawater was investigated experimentally within the QICS project. Using video footage of the CO_2 bubble plume, the dimensionless numbers, such Re and Eo, have been used for data analysis and identifying the characteristics of leaked CO_2 bubbles. The results obtained from QICS experiment were compared with results published by studying the motion of a single CO_2 gas bubble in laboratory conditions. The agreement shows with a certain variation for the drag coefficient range mainly due to the difference between the experimental conditions: laboratory and open field experiments.

The bubbles leaked from QICS experiment are the bubbles with size ranging from 2.0 to 12.0 mm in equivalent diameter and velocity from 20 cm/s to 45 cm/s, which give the Reynolds number varying from 500 to 3500, respectively. The leaked bubbles experience the break-up and coalescences. The critical break-up Eötvös

number is found to be $E_{ob} > 20$, which should be characterised by the major dimension, D_{mj}, rather than the equivalent diameter d_e.

Some observation errors generated by setting the monitoring system, such as the location of the rulers, focal blur, the plume effect and the tidal effects along with the lack of observation in three dimensions due to a single video camera was used in the experiment, can be improved by redesign the system and measuring the seawater velocity simultaneously to detect the bubble relative velocity for identifying bubble dynamics more reasonably. Additionally, Greene and Wilson (2012) suggest that an improvement on gaining the initial bubble distribution would be through an acoustic method, proved through investigating initial bubble sizes with greater accuracy than imaging methods.

The interaction between the CO_2 bubbles is a very important phenomenon to characterise analytically. The experiments with larger leakage rate would generate a plume with strong bubble interactions, from which more suitable data can be obtained for development of the suitable correlations for plume model. Future experimental work on observing the bubble interactions in different water conditions (bubble size, bubble shape, directional velocity of water and bubble, temperature, salinity) are suggested to be carried extensively in the laboratory as well, in order to develop a statistical relation of coalescence or breakup of CO_2 bubbles.

Acknowledgements

Appendix A. Supplementary data

Supplementary data associated with this article can be found, in the online version, at doi:10.1016/j.ijggc.2015.02.011.

References

Bando, S., Takemura, F., 2006. Rise speed of supercritical carbon dioxide spheres in aqueous surfactant solutions. J. Fluid Mech. 548, 133–140.

Bian, Y.C., et al., 2011. Reconstruction of rising bubble with digital image processing method. In: 2011 IEEE International Instrumentation and Measurement Technology Conference, pp. 430–435.

Blackford, J.C., Stahl, H., Bull, J.M., Berges, B.J.P., Cevatoglu, M., Lichtschlag, A., Connelly, D., James, R.H., Kita, J., Long, D., Naylor, M., Shitashima, K., Smith, D., Taylor, P., Wright, I., Akhurst, M., Chen, B., Gernon, T.M., Hauton, C., Hayashi, M., Kaieda, H., Leighton, T.G., Sato, T., Sayer, M.D.J., Suzumura, M., Tait, K., Vardy, M.E., White, P.R., Widdicombe, S., 2014. Detection and impacts of leakage from sub-seafloor Carbon Dioxide Storage. Nat. Clim. Changes 4, 1011–1016, http://dx.doi.org/10.1038/nclimate2381.

Bozzano, G., Dente, M., 2001. Shape and terminal velocity of single bubble motion: a novel approach. Comput. Chem. Eng. 25 (4–6), 571–576.

Brewer, P.G., et al., 2002. Experimental determination of the fate of rising CO_2 droplets in seawater. Environ. Sci. Technol. 36 (24), 5441–5446.

Brooks, C.S., et al., 2012. Two-group drift-flux model for closure of the modified two-fluid model. Int. J. Heat Fluid Flow 37, 196–208.

Chen, B.X., et al., 2005. Modeling near-field dispersion from direct injection of carbon dioxide into the ocean. J. Geophys. Res. – Oceans 110 (C9).

Chen, B., et al., 2009. The fate of CO_2 bubble leaked from seabed. Energy Procedia 1 (1), 4969–4976.

Chun, B.-S., Wilkinson, G.T., 1995. Interfacial tension in high-pressure carbon dioxide mixtures. Ind. Eng. Chem. Res. 34 (12), 4371–4377.

Clift, R., Grace, J., Weber, M., 1978. Bubbles Drops and Particles, New York.

Dewar, M., et al., 2013. Small-scale modelling of the physiochemical impacts of CO_2 leaked from sub-seabed reservoirs or pipelines within the North Sea and surrounding waters. Mar. Pollut. Bull. 73 (2), 504–515.

Dewar, M., et al., 2014. Dynamics of rising CO_2 bubble plumes in the QICS field experiment. Part 2 – modelling. Int. J. Greenh. Gas Control, http://dx.doi.org/10.1016/j.ijggc.2014.11.003.

Domingos, M.G., Cardoso, S.S.S., 2013. Turbulent two-phase plumes with bubble-size reduction owing to dissolution or chemical reaction. J. Fluid Mech. 716, 120–136.

Freund, P., Ormerod, W.G., 1997. Progress toward storage of carbon dioxide. Energy Convers. Manag. 38 (Supplement), S199–S204.

Greene, C.A., Wilson, P.S., 2012. Laboratory investigation of a passive acoustic method for measurement of underwater gas seep ebullition. J. Acoust. Soc. Am. 131, EL61–EL66.

Han, J.-H., et al., 2012. Optimal strategy for carbon capture and storage infrastructure: a review. Korean J. Chem. Eng. 29 (8), 975–984.

Hongyi, W., Feng, D., 2009. Geometric method for bubble volume computing based on high-speed image. In: Instrumentation and Measurement Technology Conference, I2MTC '09, IEEE, 2009.

Ito, M., 1984. Chemical Handbook, 3rd ed. The Chemical Society of Japan, s.l.:Maruzen Publishing Company, Tokyo.

Kelbaliyev, G.I., 2011. Drag coefficients of variously shaped solid particles: drops, and bubbles. Theor. Found. Chem. Eng. 45 (3), 248–266.

Liao, Y.X., Lucas, D., 2009. A literature review of theoretical models for drop and bubble breakup in turbulent dispersions. Chem. Eng. Sci. 64 (15), 3389–3406.

Luke, A., Cheng, D.C., 2006. High speed video recording of bubble formation with pool boiling. Int. J. Therm. Sci. 45 (3), 310–320.

Luther, S., Rensen, J., Guet, S., 2004. Bubble aspect ratio and velocity measurement using a four-point fiber-optical probe. Exp. Fluids 36 (2), 326–333.

Marchetti, C., 1977. On geoengineering and the CO_2 problem. Clim. Change 1 (1), 59–68.

National Bureau of Standards (NBS), 1960. Tables of Thermodynamic and Transport Properties of Air, Argon, Carbon Dioxide, Carbon Monoxide, Hydrogen, Nitrogen, Oxygen and Steam. Pergamon Press, Oxford.

Noble, R.R.P., et al., 2012. Biological monitoring for carbon capture and storage – a review and potential future developments. Int. J. Greenh. Gas Control 10, 520–535.

Rodrigue, D., 2001. Drag coefficient-Reynolds number transition for gas bubbles rising steadily in viscous fluids. Can. J. Chem. Eng. 79 (1), 119–123.

Schetz, J.A., Fuhs, A.E., 1999. Fundamentals of Fluid Mechanics. John Wiley & Sons.

Schneider, C.A., Rasband, W.S., Eliceiri, K.W., 2012. NIH Image to ImageJ: 25 years of image analysis. Nat. Methods 9, 671–675.

Sommerfeld, M., Wirth, K.-E., Muschelknautz, U., 2010. L3 two-phase gas–solid flow. In: VDI Heat Atlas. Springer, Berlin, Heidelberg, pp. 1181–1238.

Takemura, F., Yabe, A., 1999. Rising speed and dissolution rate of a carbon dioxide bubble in slightly contaminated water. J. Fluid Mech. 378, 319–334.

TradeXchange, C., 2013. Carbon Trade Exchange C. TradeXchange, Editor.

Unesco, 1981. Tenth Report of the Joint Panel on Oceanographic Tables and Standards. Unesco Technical Papers in Marine Science, vol. 36., pp. 24–29.

Wang, H.Y., Dong, F., 2008. Track of rising bubble in bubbling tower based on image processing of high-speed video. In: Fang, J., Wang, Z. (Eds.), Seventh International Symposium on Instrumentation and Control Technology: Optoelectronic Technology and Instuments, Control Theory and Automation, and Space Exploration.

Wang, H.Y., Dong, F., 2009. A method for bubble volume calculating in vertical two-phase flow in The 6th International Symposium on Measurment Techniques for Multiphase Flows. J. Phys. Jpn.

Zaruba, A., et al., 2005. Experimental study on bubble motion in a rectangular bubble column using high-speed video observations. Flow Meas. Instrum. 16 (5), 277–282.

Zhang, L., Yang, C., Mao, Z.S., 2008. An empirical correlation of drag coefficient for a single bubble rising in non-Newtonian liquids. Ind. Eng. Chem. Res. 47 (23), 9767–9772.

Zhang, X., et al., 2012. Experimental study on gas holdup and bubble behavior in carbon capture systems with ionic liquid. Chem. Eng. J. 209, 607–615.